▌Magnetic Properties

Rational Design of Lanthanoid Single-Ion Magnets: Predictive Power of the Theoretical Models

José J. Baldoví,[a] Yan Duan,[a] Roser Morales,[b] Alejandro Gaita-Ariño,[a] Eliseo Ruiz,*[b] and Eugenio Coronado*[a]

Abstract: We report two new single-ion magnets (SIMs) of a family of oxydiacetate lanthanide complexes with D_3 symmetry to test the predictive capabilities of complete active space ab initio methods (CASSCF and CASPT2) and the *semiempirical* radial effective charge (REC) model. Comparison of the theoretical predictions of the energy levels, wave func-
tions and magnetic properties with detailed spectroscopic and magnetic characterisation is used to critically discuss the limitations of these theoretical approaches. The need for spectroscopic information for a reliable description of the properties of lanthanide SIMs is emphasised.

Introduction

The magnetism of lanthanides has intrigued researchers for decades. This interest increased with the discoveries, first in solid state and then in the field of molecular magnetism, of 4f ion mononuclear complexes presenting slow relaxation of the magnetisation, that is, with single-molecule magnet (SMM) behaviour.[1,2] In the past decade, the impact of mononuclear SMMs, also known as single-ion magnets (SIMs), has dramatically increased.[3–5] This type of molecular compound exhibits attractive physical properties such as magnetic hysteresis at low temperatures and quantum phenomena.[6,7]

In contrast to the first generation of SMMs discovered in the 1990s[8]—magnetic clusters, the properties of which rely on the ability of exchange interactions to stabilise anisotropic high-spin states—the magnetic and quantum properties of mononuclear SMMs, which are the second generation of SMMs, depend primarily on the anisotropy of a single ion. In lanthanides, the spin–orbit coupling is one order of magnitude stronger than the crystal field splitting. Thus, the magnetic anisotropy is determined by the electrostatic interaction between the f-electrons and the ligand electrons, resulting in the splitting of the ground J into $2J+1$ microstates. For the study of the optical properties of lanthanide complexes, the spectro-scopic energy levels are commonly analysed by the determination of the symmetry-allowed crystal-field parameters (CFPs) by a direct fit of UV–visible spectroscopic experimental data.[9] In the absence of spectroscopic data or when dealing with non-ideal chemical structures, this approach usually results in over-parameterisation. Modelling the properties of f-element complexes remains an open problem in molecular magnetism, where the majority of lanthanide coordination compounds are low-symmetry and are routinely characterised only by thermodynamic measurements (magnetometry). More recently, it has been demonstrated that a full experimental determination of the CFPs that describes the low-lying magnetic levels is possible by performing a combination of different experimental techniques,[10] such as far infrared (FIR),[11] inelastic neutron scattering spectroscopy (INS),[12] high-resolution luminescence, magnetic circular dichroism (MCD) and electron paramagnetic resonance (EPR) spectroscopies. Such spectroscopic techniques have been combined with cantilever torque magnetometry,[13] providing an accurate description of the crystal field splitting of the polynuclear lanthanide SMM Dy_3.[14] However, this phenomenological approach cannot be used to guide the synthesis of new derivatives exhibiting SMM behaviour, as experimental measurements are performed once the compound has been synthesised and its theoretical characterisation is provided a posteriori.

From the computational point of view there are a few alternatives to calculate the CFPs and predict the spectroscopic and magnetic properties of f-block SIMs.[15] The simplest procedure is based on the point charge electrostatic model (PCEM),[16] subsequently improved by several *semiempirical* models.[17–22] These models, while very useful for quick predictions of the properties and for obtaining an initial set of CFPs, also need parameterisation to take into account covalency to provide a more realistic description of the observed properties of the system. A more expensive approach involves the calculation of the energy levels using electronic structure ab initio

[a] Dr. J. J. Baldoví, Y. Duan, Dr. A. Gaita-Ariño, Prof. E. Coronado
Instituto de Ciencia Molecular (ICMol)
Universidad de Valencia, C/Catedrático José Beltrán 2
46980 Paterna (Spain)
E-mail: eugenio.coronado@uv.es

[b] R. Morales, Prof. E. Ruiz
Departament de Química Inorgànica and
Institut de Recerca de Química Teòrica i Computacional
Universitat de Barcelona, Diagonal 645, 08028 Barcelona (Spain)
E-mail: eliseo.ruiz@qi.ub.es

▤ Supporting information for this article is available on the WWW under http://dx.doi.org/10.1002/chem.201601741; including details of the experimental measurements and the theoretical calculations.

These are not the final page numbers! ↗↗

methods. In general, this last approach has practically been the default option for the theoretical characterisation of SIMs as first principles methods are expected to be more exact compared with the more intuitive electrostatic methods.[23–25] However, when spectroscopic techniques are used to determine the energy levels, evidence of important deviations between the theoretical predictions, obtained by these methods with the experiment have been accumulating recently.[11,12,26] While both electrostatic and ab initio methods are nowadays considered standard tools in the field of molecular magnetism, there is a lack of benchmark studies to critically compare their performance in the modelling and rational design of lanthanoid SMMs. Thus, the study of their limitations and the analysis of their pros and cons is a general requirement in the field. To advance in this direction we should take a magnetic molecule where the energy levels have already been measured by high-quality spectroscopic experiments, blindly "predict" the energy level scheme using the two kinds of theoretical models and, finally, compare the spectroscopic and magnetic experimental properties with the theoretical predictions. An interesting study along this direction has been performed by using SQUID magnetometry and INS measurements,[11] as well as the work of Marx et al.[10] where far IR and INS spectroscopies were employed. Nevertheless, these works did not deeply analyse the reported divergences between theory and experiment. The only effort to try to approach the experiment has been to introduce scaling factors in these models without any proper justification.

In this work we have used the series $Na_5[Ln(oda)_3](H_2O)_6(BF4)_2$, where $Ln = Dy^{III}$, Er^{III} and oda = oxydiacetate ($C_4H_4O_5^{2-}$), in short DyODA and ErODA, respectively, as test systems to compare the capabilities of these two kind of theoretical models in lanthanoid SMMs. We selected these two isostructural compounds because of the availability of a combination of spectroscopic measurements and the fact that their calculated ground doublet wave functions suggested they could exhibit SMM behaviour.[27,28] In the first part, we performed an experimental magnetic characterisation of the compounds, checking for slow relaxation of the magnetisation. Then, in the second part we applied different levels of ab initio and effective electrostatic calculations to discuss their ability to predict the experimental spectroscopic and magnetic information.

Experimental Section

The syntheses of DyODA and ErODA were performed by following a previously described procedure.[29] All reagents were commercially purchased and used without any further purification. $DyCl_3·6H_2O$ and $ErCl_3·6H_2O$ are highly hygroscopic and were stored in a desiccator. After the syntheses, pure block-shaped colourless crystals of DyODA and pure block-shaped pink crystals of ErODA were obtained by recrystallisation of the crude sample in a minimum amount of milli-Q water.

The compounds were characterised by FT-IR spectroscopy (Figures S1 and S2 in the Supporting Information), X-ray power diffraction

and single-crystal X-ray diffraction. The unit cell parameters are coincident with the ones reported previously[29] (Figures S3 and S4). IR spectra were recorded on an FT-IR Nicolet 5700 spectrometer in the 2000–400 cm^{-1} range by using powdered crystals in KBr pellets. For DyODA (Figure S1 in the Supporting Information), FT-IR spectroscopy data in the range 2000–400 cm^{-1} (KBr pellet): 1622(s), 1459(s), 1423(s), 1362(s), 1317(s), 1247(m), 1126(s), 1084(s), 1047(s), 959(m), 935(s), 709(m), 604(w), 571(m), 534(w), 522(s). For ErODA (Figure S2), FT-IR spectroscopy data in the range 2000–400 cm^{-1} (KBr pellet): 1620(s), 1427(s), 1366(s), 1320(s), 1124(m), 1050(s), 958(m), 935(s), 710(m), 609(w), 571(m), 523(w).

Polycrystalline samples of both derivatives were lightly ground in an agate mortar and pestle and filled into 0.7 mm borosilicate capillaries prior to being mounted and aligned on a Empyrean PAN analytical powder diffractometer, using $Cu_{K\alpha}$ radiation ($\lambda = 1.54056$ Å). For each sample, three repeated measurements were collected at room temperature ($2\theta = 2$–$40°$) and merged in a single diffractogram. For both compounds, powder-XRD verified that the bulk samples consist of a single phase, which corresponds to the crystal structures (as shown in Figures S3 and S4 in the Supporting Information).

Magnetic susceptibility, χ_m, data were measured between 2 and 300 K with a commercial magnetometer equipped with a SQUID sensor and a commercial physical properties measurement system (PPMS). The diamagnetic contributions to the susceptibility were corrected using Pascal's constant tables. Static (dc) magnetic data were collected with an applied field of 1000 Oe and also without field. Alternate current (ac) data were collected in the range 2–10 K with an applied dc field of 1000 Oe at different frequencies in the range 1500–10000 Hz.

For the theoretical characterisation of the spectroscopic and magnetic properties, we used two well-established theoretical approaches: complete active apace ab initio calculations[30] and the semiempirical electrostatic method based on radial effective charge (REC) model.[22]

For the electronic structure ab initio study, we performed post-Hartree–Fock calculations based on the relativistic quantum chemistry method CASSCF + RASSI implemented in the MOLCAS 8.0 software package for DyODA and ErODA.[31] The active space of the CASSCF method included nine electrons in seven orbitals and eleven electrons in seven orbitals, for DyODA and ErODA, respectively. The employed CASSCF is limited to the 4f electrons and orbitals, as is the standard procedure in the field. CASSCF calculations were performed for three different multiplicities (sextet, quartet and doublet) for the Dy complex, and two multiplicities (quartet and doublet) for the Er complex. We included 21, 128 and 98 states for the sextet, quartet and doublet calculations of the Dy complex. While for the Er derivative we included 35 and 112 states for the quartet and doublet calculations. In the case of the CASPT2 calculations of the ground state multiplicities, we included 21 states for the sextet of Dy and 13 states for the quartet of Er. The effect of spin-orbit coupling on the basis of the converged wave functions obtained in the previous step (CASSCF or CASPT2) is included by the restricted active space state interaction (RASSI) method. Spin Hamiltonian parameters (such as g factors) can be calculated from the wave functions resulting after the state interaction step employing the SINGLE_ANISO program, implemented in MOLCAS 8.0. The employed basis set has the following contractions: Dy [9s8p6d4f3g2h]; Er [9s8p6d4f3g2h]; O close [4s3p2d1f]; O distant [3s2p]; C [3s2p]; H [2s]. The structure of the model was extracted from the corresponding X-ray structure without any ligand simplification. Electrostatic potential maps were obtained by B3LYP calculations as implemented in Gaussian 09[32] using a TZVP basis set

↖↖ **These are not the final page numbers!**

employing the geometry for the ligand environment of the previous CASSCF+RASSI calculations and removing the central Dy^{III} or Er^{III} ion.

For the REC calculations, we used the SIMPRE computational package.[33] In a first step the radial effective charge (REC) model[22] was applied to the crystallographic coordinates of the first coordination sphere of DyODA and ErODA (see the Supporting Information for details). The REC model is an electrostatic model that considers the effect of the coordinated atoms (X) through effective point charges located in the lanthanide–ligand axis at an effective distance R_{eff}. Such an effective distance is equal to $r_i - D_r$, where r_i is the distance between the atomic positions of the lanthanide and the donor atom (Figure 1).
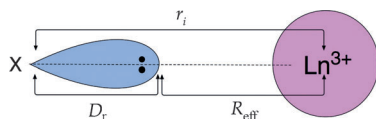

Figure 1. Electronic pair of a ligand X oriented towards the nucleus of a trivalent lanthanoid cation. The effective charge is located between the lanthanoid and the donor atom $R_{eff} = r_i - D_r$.

Oxygen donor atoms from oxydiacetate-type ligands—neither carboxylate nor ether—have not been parameterised before by the REC model. Hence, if we want to provide an inexpensive prediction of the energy levels, wave functions, g components, magnetic susceptibility and magnetisation of the lanthanide oxydiacetate complexes, we can take advantage of a relation that was obtained recently by fitting the experimental energy levels of the ground multiplet of the homoleptic families, CsNaYCl$_6$:Ln^{III} and CsNaYF$_6$:Ln^{III}, LiYF$_4$:Ln^{III} and LaCl$_3$:Ln^{III} using the crystal structures and the REC model.[34] This approximation permits the calculation of the effective distances of the coordinated atoms using the following *semi-empirical* formula for D_r:

$$D_r \approx \left(\frac{N_L}{V_M}\right) \frac{1}{E_M(E_L - E_M)} \tag{1}$$

where N_L is the coordination number of the complex ($N_L = 9$), V_M is the valence of the metal ($V_M = 3$), and E_M and E_L are the Pauling electronegativities of the metal ($E_M = 1.22$ and $E_M = 1.24$ for Dy and Er, respectively) and the donor atom ($E_L = 3.44$ for oxygen), respectively. Regarding the effective charges of the donor atoms, it could be estimated, assuming the same relation $f = Z_i \times D_r$, that the obtained using the two REC parameters of two series of polyoxotungstate single-ion magnets ($f = 0.094$), which were recently modelled and added to the general library of the model, predicting slow relaxation of the magnetisation in a Nd^{III}-based SIM.[35] This strategy allowed us to obtain a quick estimation of the ground multiplet spectroscopic and magnetic properties in the absence of any parameter, by just utilising the previous knowledge in the study of the properties of lanthanide homoleptic coordination compounds. Thus, all the calculations presented in this study are predictions, as we aimed to compare the performance of these theoretical approaches to model the magnetic and spectroscopic properties of lanthanoid SIMs. For comparison, the REC model was also used by the usual procedure of fitting of the experimental data in order to add carboxylate and ether ligands to the library (details are in the Supporting Information and the results concerning energy levels are represented in Figures S14–S17 and magnetic properties in Figures S18 and S19).

Results and Discussion

Structure

The crystal structures of both compounds have been previously described in detail.[29] Both compounds undergo spontaneous resolution on crystallisation. The central lanthanide ion coordinates three oxydiacetate anions to form a nine-coordinate complex anion, [Ln(oda)$_3$]$^{3-}$. With a coordination geometry around the lanthanide ion that can be described as distorted three-face centred trigonal prismatic, two possible helical Δ/Λ chiralities result for the [Ln(oda)$_3$]$^{3-}$ anion (Figure 2). The crystal structure can be refined in one of the Sohncke space groups (R32).

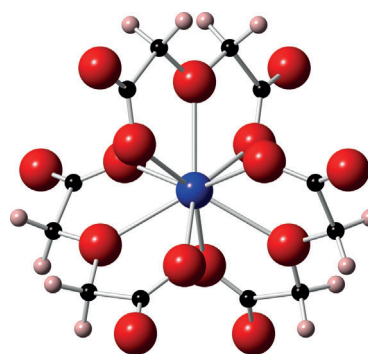**Figure 2.** Vertical view of the three-blade-propeller molecular structure of Na$_5$[Dy(oda)$_3$](H$_2$O)$_6$(BF$_4$)$_2$ that emphasises the near-C_3 symmetry axis. The erbium derivative is isostructural.

It has been reported[29] that the formation of hydrogen bonds involving BF$_4^-$ anions could be essential in the packing of the homochiral complexes, resulting in the spontaneous resolution. The coordination geometry around the lanthanide ion is practically identical for both DyODA and ErODA. It may be described as slightly distorted tricapped trigonal prismatic (of D_3 symmetry), with the upper and lower triangles defined by carboxylate oxygen atoms and the capping positions (perpendicular to the near-C_3 symmetry axis) occupied by ether oxygen atoms. Thus, the coordination environment is neither clearly axial nor equatorial,[36] and therefore it is necessary to perform structure-based theoretical calculations to know which lanthanide ion is a better candidate to exhibit SMM behaviour.

Magnetic properties

The dc susceptibility measurements were performed for the pure and diluted samples of both compounds (Y$_{(1-x)}$Ln$_{(x)}$ with $x = 0.01$ for Dy, $x = 0.05$ for Er) under an applied field of 0.1 T. The $\chi_m T$ values at 300 K are near the expected values for the $^4I_{15/2}$ and $^6H_{15/2}$ multiplets of Er^{III} (11.27 (exp.) vs. 11.48 emu K mol^{-1}) and Dy^{III} (14.08 (exp.) vs. 14.17 emu K mol^{-1}). To avoid dipolar interactions that are not included in both theoretical calculations, the experimental $\chi_m T$ products of the diluted sam-

These are not the final page numbers! ↗↗

ples of DyODA and ErODA are compared with the theoretical results in Figure 3. It can be seen that the temperature-dependent magnetic susceptibility gradually decreases upon cooling due to depopulation of the electronic fine structure, reaching values close to 6 emu K mol^{-1} for both complexes.
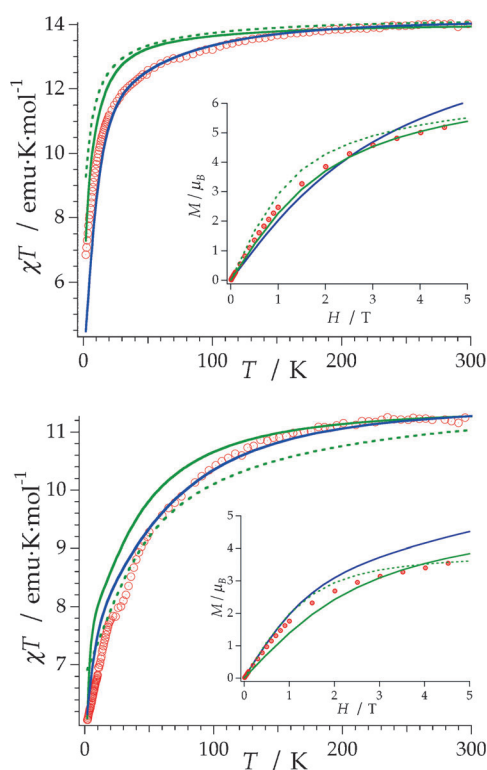

Figure 3. Comparison of the $\chi_m T$ product for the magnetically diluted powder samples of $Y_{0.99}Dy_{0.01}ODA$ (top) and $Y_{0.95}Er_{0.05}ODA$ (bottom) at $H = 1000$ Oe. Inset: magnetisation at 5 K of $Y_{0.99}Dy_{0.01}ODA$ (top) and $Y_{0.95}Er_{0.05}ODA$ (bottom). Red open circles: experiment; blue solid line: REC prediction; green solid line: CASSCF, green dashed line: CASPT2.

The overall shape of both experimental curves is well reproduced by all three methods (REC prediction, CASSCF and CASPT2 results). It is remarkable that the electrostatic method (blue solid line) reproduces the $\chi_m T$ curves with an almost excellent agreement with the experiment (red open circles) in both cases. In the case of the ab initio calculated $\chi_m T$ product there is no improvement between CASSCF and CASPT2, both being almost equivalent in the Dy derivative except at low temperature. There are noticeable differences between CASSCF (green solid line) and CASPT2 (green dashed line) in the Er example (Figure 3, bottom), where CASPT2 seems to reproduce better the magnetic behaviour below 100 K, while at higher temperatures CASSCF is closer to the experiment. Dynamic correlation contribution seems to be more important for the erbium system, probably for the larger electron repulsion due to the presence of two extra electrons in the f orbitals in comparison with the Dy complex. In any event, the CASSCF method provides reasonable values, as expected, taking into account the relatively large ionic character of the metal–ligand interactions. In particular, CASPT2 calculations predict $\chi_m T =$

11.03 emu K mol^{-1}, which may indicate a higher total crystal field splitting than the one obtained by the CASSCF method. In addition, the temperature-dependent magnetic susceptibility of DyODA and ErODA has been calculated by using the CFPs from references [27] and [28] in the CONDON computational package[37] showing an almost perfect agreement with the experiment (Figures S20 and S22 in the Supporting Information).

Regarding the magnetisation, one can observe that for the ground state the magnetic properties seem to be better reproduced using the most sophisticated methods. In both cases, the shape of the magnetisation curve predicted by ab initio methods coincides better with the experimental behaviour, although the improvement of using CASPT2 is still not evident and generalisable: with ErODA CASPT2 results are clearly superior to those obtained using CASSCF, but the contrary is observed with DyODA. This is related with the better reproduction of the magnetic susceptibility at low temperature in the case of CASSCF (Figure 3, top, green solid line) compared with CASPT2 (Figure 3, bottom, green dashed line). The magnetisation calculated using the phenomenological CFPs from reference [27] and [28] were plotted versus the experimental data in Figures S21 and S23 in the Supporting Information, for DyODA and ErODA, respectively. In the case of DyODA, the calculated curve is very similar to the one predicted by the REC model, whereas a better reproduction of the experimental results is given for ErODA.

On the other hand, considering the information of the magnetic susceptibility between 2 and 300 K, the better agreement of the electrostatic calculation with the experiment allows us to assume that, in these two particular examples, the energy level scheme should also be better reproduced by the *semiempirical* method. In the next section, we take advantage of spectroscopic data in order to compare both approaches with the experimental energy level schemes for these two complexes and elucidate this question (Figure 5 and Figure 6).

The ac susceptibility measurements were performed for both compounds above 2 K. In both cases, they reveal the typical features associated with the SMM behaviour for a system with some mixture of M_J components enabling the possibility of presenting avoided hyperfine crossings and quantum tunnelling. Hence, in the absence of a dc field there is a weak frequency-dependent signal in χ'' but no clear χ' signal (Figure S5, left, in the Supporting Information). The system is taken beyond the hyperfine crossing region after applying an external field of 1000 Oe. As a result, both χ' and χ'' show strong frequency dependencies. This indicates the presence of a slow relaxation process involving an energy barrier for the reversal of the magnetisation. In the Dy derivative, a maximum is detected between 2.5 and 3.0 K in χ' (Figure 4, top, left), which is frequency dependent. In χ'', the maximum could not be observed in the measurements carried out between 2 and 10 K (Figure 4, bottom, left). The upward trend from 4 to 2 K permits the expectation that the position of the maximum should appear between 1 and 2 K, but this is outside our operating range. On the other hand, the magnetic properties of ErODA reveal the typical features associated with SMM behaviour.

↖↖ These are not the final page numbers!

Thus, both χ' and χ'' under an applied magnetic field of 1000 Oe (Figure 4, right) show strong frequency dependencies, which indicates the presence of a slow relaxation process involving an energy barrier for the reversal of the magnetisation. Depending on the frequency of the applied ac field, χ' presents a maximum between 4.3 and 4.9 K, while χ'' has also a maximum between 3.5 and 4.2 K for 1500 and 10 000 Hz, respectively (Figure 4, right, bottom). Dynamic susceptibility measurements under an alternating field for the diluted ErODA compound are presented in Figure S6. Arrhenius analysis was performed, which, as reported in the Supporting Information (Figure S7), results in an effective barrier of 31 cm^{-1}. As discussed in the next section, spectroscopic information allows us to discard this effective barrier as an artefact.
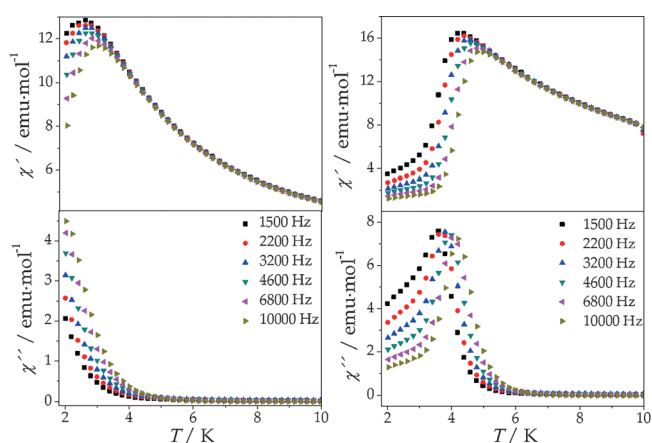

Figure 4. In-phase (top) and out-of-phase (bottom) dynamic susceptibility of DyODA (left) and ErODA (right) under an applied dc field of 1000 Oe at the frequencies shown in the legend.

Theoretical analysis using the energy level scheme

In references [27] and [28], a large number of energy levels were located and assigned for both members of the LnODA family (65 for Er, 152 for Dy) by a combination of spectroscopic techniques, which in both studies consisted of optical absorption (unpolarised, linearly and circularly polarised), and was also extended to optical emission (also including all polarisations) for DyODA. Fits assumed a trigonal CF symmetry, thus in each case six CF parameters (B_2^0, B_4^0, B_6^0, B_4^3, B_6^3 and B_6^6) were varied in order to find a complete description of the experimental properties. In both derivatives, the root-mean-square deviation between the fit and the experimental data is below 10 cm^{-1} for the whole spectrum, and below 7 cm^{-1} for the ground J manifold, so this is the expected accuracy for the missing experimental levels in the case of the erbium derivative. Note that this accuracy is maintained for energies in the tens of thousands of cm^{-1}, accounting for the power of this approach and justifying its use as benchmark or "gold standard" to judge the quality of theoretical calculations when not all the experimental energy levels are available. The phenomenological CFPs extracted from the fit in references [27] and [28] are reported together with the predicted ones by CASSCF

and the REC model in the Supporting Information. The CFPs predicted by the REC model are very close to the phenomenological ones for both derivatives. The wave functions and g components of the ground state, as well as the input coordinates used in both calculations are also included. One can observe that in the case of DyODA, the values of g_z are very similar between CASSCF (13.1), CASSPT2 (15.8) and REC (14.4), whereas there is a strong change in the magnetic moment of the ground state of the Er complex when passing from CASSCF ($g_z = 2.0$) to CASPT2 ($g_z = 14.5$). A possible explanation for this could be the presence of a larger number of electrons in the f shell. Hence, dynamic correlation effects become more important and they are perturbative only in the CASPT2 method. The REC model predicts $g_z = 10.8$, which is also compatible with the observed SMM behaviour.

In Figure 5 (DyODA) and Figure 6 (ErODA), we compare these reference data with different sets of theoretical energy levels using the real structures of both complexes, by three different strategies. We have to stress that, in this case, the application of the REC model does not rely on any free-fitting parameters, as we explained in the Experimental Section.
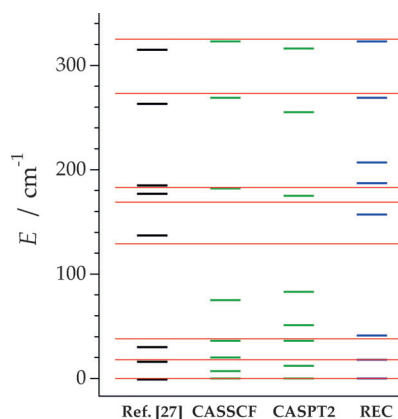

Figure 5. Crystal field energy level scheme of the ground J multiplet of DyODA. Thin red lines: experimental optical spectrum. Thick lines: spectroscopic fit (reference [27]), CASSCF/CASPT2 energies including spin-orbit effects and REC model prediction, as indicated at the axis (details in the text).

The experimental energy level scheme of DyODA can be described as a "bunching" of levels in three groups 3+3+2, where each group has a width of about 50 cm^{-1} and there is a gap with no levels of about 80 cm^{-1} between each two groups. This 3+3+2 description is well reproduced by the *semiempirical* REC prediction. In contrast, both CASSCF and CASPT2 respond rather to a 5+1+2 scheme, that is, the fourth and fifth energy levels, that experimentally are found near 150 cm^{-1}, are predicted to be about 50 % lower in energy, around 75 cm^{-1}. The total energy level splitting, of about 320 cm^{-1}, is adequately reproduced by all methods. The CASPT2 method improves CASSCF results for the low lying state energies that are crucial for the theoretical determination of the anisotropy barriers. On the other hand, the prediction provided by the REC model using Equation (1) offers a remarkable reproduction of the scheme, as confirmed in the correct

These are not the final page numbers! ↗↗

prediction of the $\chi_m T$ product. In addition, one can observe that following this methodology the total CF splitting is perfectly determined and the scheme $3+3+2$ is also obtained. This is not trivial, as different values of R_{eff} will modify the ratio between the 2nd-, 4th- and 6th-rank parameters, changing the levels distribution. In this particular case, this predictive electrostatic approach results in a very satisfactory description of the energy levels.
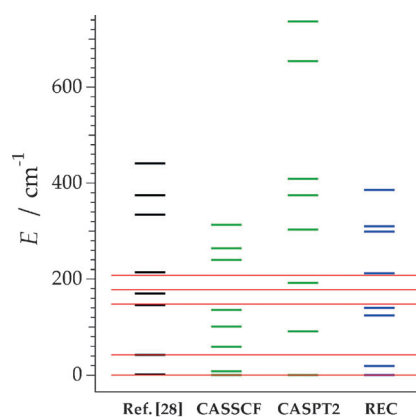

Figure 6. Crystal field energy level scheme of the ground J multiplet of ErODA. Thin red lines: experimental optical spectrum. Thick lines: fit (reference [28]), CASSCF/CASPT2 energies including spin-orbit effects and REC model prediction, as indicated at the axis (details in the text).

For the Er derivative, five of the eight CF Kramers doublets to split out of the $^4I_{15/2}$ (ground) multiplet were reported.[28] Taking the spectroscopic fit as a reference for the whole set of levels (black thick line in Figure 6), a slightly different $2+3+3$ bunching is observed, with bunches that are at the same time increasingly wider (40, 70 and 110 cm^{-1}) and more separated than in the Dy case (over 100 cm^{-1} for each of the interbunch separation).

In this case, the CASSCF calculation qualitatively predicts the $2+3+3$ bunches, but underestimates all energies, so that in general the CASSCF levels are situated in the energies between the experimentally found energy bunches. Interestingly, while in this case an overall increase in CASSCF energies of about 50 % would improve the agreement, the factor would be of the order of 400 % if only the first excited state is considered, highlighting the risk of using these factors with partial information, as it was done in references [12] and [26]. As reflected in the $\chi_m T$ curve (Figure 3, bottom) in the case of CASPT2 the difference between the calculated energy levels with respect to CASSCF is striking, but also far from the experimental result with no clear improvement. In this case, a $1+6+2$ bunching is found with a total splitting of about 740 cm^{-1}, which is a 68 % higher than the results of the phenomenological fit (441 cm^{-1}). Such a total splitting seems unreasonable and is key to understanding the deviation of the $\chi_m T$ product with respect to the experiment (Figure 3, bottom, green dashed line). On the other hand, the REC prediction is not as accurate as the one calculated in DyODA, but still respects the $2+3+2$ scheme. The total splitting calculated by the REC model is very close to the one calculated with the phenomenological fit and thus is expected to be close to the actual energy levels.

As mentioned in the previous section, the magnetic data suggest an Orbach mechanism, but in this case we can positively discard that a relaxation via an excited state happens at 31 cm^{-1}, since the spectroscopy determines the first excited state to be at 40 cm^{-1} (Figure 6). It is important to note that it has been very common in this field to assume an Orbach process without proof and without spectroscopic information to back it up. Furthermore, by inspecting the typical errors of CASSCF, CASPT2 and the REC model, it is easy to see that sometimes the experimental effective barrier will, by mere chance, be in the range of a theoretical prediction, giving an appearance of confirmation. Moreover, while in some cases the Arrhenius plot displays some curvature, pointing to other relaxation pathways (Raman, quantum tunnelling or a direct process), no signs of this can be found in the case of ErODA. It is to be expected that in a number of cases an Orbach mechanism has been mistakenly proposed, either by default or even with an appearance of theoretical confirmation, and only spectroscopic information will eventually allow correcting these errors.

Limitations of CASSCF, CASPT2 and the REC model

After analysing these two particular examples, let us critically review general limitations of ab initio calculations and the electrostatic approach. For clarity, let us first briefly enumerate the limitations of each approach, and then go into some detail. In this regard, complete active space ab initio calculations:

1) consider a single complex (the results should be compared with those obtained with magnetically dilute samples)
2) apply perturbations in the wrong order, in CASPT2 both dynamic correlation and spin-orbit effect are included perturbatively
3) are limited by large computational requirements that impede the expansion of the active space beyond the seven 4f orbitals; this should be the pathway to increase the accuracy.

Even when more than a single metal is considered, dipolar interactions within the crystals are also outside the scope of this approach. More crucially, the fact that the SINGLE_ANISO procedure applies spin–orbit coupling after, rather than before, the ligand field, has fundamental, limiting consequences in the accuracy of the method that have not yet been adequately evaluated. On top of that, there are the non-fundamental limits posed by large computational requirements, especially in the case of the CASPT2 method. Because it is a computationally demanding method, it could be that the end results have not converged. Hence, using a larger basis set, changes in the basis contractions or increasing the active space would produce results that are closer to the experimental data. Again, an extra theoretical effort will eventually overcome point (2), but it will require programming new calculation procedures. However, electronic structure methods provide several useful

↖↖ These are not the final page numbers!

pieces of information (g components, energy of the states, probability of the different spin relaxation mechanism between states and so on) and tools for understanding the magnetic properties (electrostatic potential of the ligands, shape of the electron density).

The *semiempirical* REC model considers:

1) a single metal
2) the first coordination sphere
3) the ground *J* multiplet
4) it is a parametric (*semiempirical*) method that often relies on low-quality data (powder $\chi_m T$) and assumes that parameters are reusable.

As it considers a single metal, this method is inappropriate for cluster-type complexes. Limiting the point charges to the first coordination sphere can have severe consequences for the prediction of the easy axis of magnetisation, while limiting the treatment to the ground *J* means the upper levels, even within the ground *J*, are less well described, and their energies are often overestimated. Being *semiempirical* means there is no systematic method to obtain more accurate CF parameters, other than fitting higher-quality (spectroscopic) experimental data. That includes the risk of assuming that parameters extracted from a compound can be used on a different one. Some of these points can be improved by extra theoretical effort. For example point (3), is solved by considering the full single-ion Hamiltonian (e.g., using the REC parameters in the CONDON computational package),[37] while point (4) is continuously being improved as the number of examples studied by this method grow, which provide a better understanding of the adequate parameterisation of each kind of ligand.

Finally, as expected, the spectroscopic fit offers a perfect description of the measured levels. Nevertheless, it is important to point out that such a phenomenological approach can only be carried out after the energy level scheme is properly determined and it is only adequate when the symmetry of coordination environment is comparable to a point group, thus reducing the number of CF parameters. Most of the coordination complexes of interest in molecular magnetism present coordination environments that provide 27 non-negligible crystal field parameters, and thus require models based on the prediction of the properties from the real structure, such as the two approaches that have been compared and discussed here, which can be understood as complementary.[38]

Conclusions

In this work we have successfully used spectroscopic information from previous studies to anticipate the SMM behaviour of the dysprosium and erbium derivatives of an oxydiacetate complex series. Their magnetic properties under ac and dc fields were experimentally determined, and for their study we performed different state-of-the-art theoretical calculations to evaluate and compare their predicting capabilities. Taking the magnetic measurements performed in this work together with the spectroscopic transition data as a reference, one needs to

conclude that current complete active space ab initio methods can offer a reasonable reproduction of the magnetic properties of both compounds, but fail to account for the energy-level distribution, including the energy of the first excited state. In this sense, there is no clear benefit for all cases in the extra computational cost of using more sophisticated models, that is, for these tasks CASPT2 does not prove to be superior to CASSCF and CASSCF is not superior to REC. In these two examples, the simple electrostatic REC model offers an inexpensive tool to obtain a promising initial prediction of CFPs, energy levels and magnetic properties. Note, however, that this is a rather favourable case for REC model, with a near-homoleptic coordination sphere which enhances its predictive character.
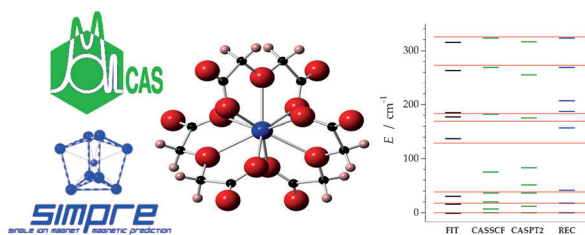
[1] R. Giraud, W. Wernsdorfer, A. M. Tkachuk, D. Mailly, B. Barbara, *Phys. Rev. Lett.* **2001**, *87*, 057203.
[2] N. Ishikawa, M. Sugita, T. Ishikawa, S. Koshihara, Y. Kaizu, *J. Am. Chem. Soc.* **2003**, *125*, 8694–8695.
[3] M. A. AlDamen, J. M. Clemente-Juan, E. Coronado, C. Marti-Gastaldo, A. Gaita-Ariño, *J. Am. Chem. Soc.* **2008**, *130*, 8874–8875.
[4] S.-D. Jiang, B.-W. Wang, G. Su, Z.-M. Wang, S. Gao, *Angew. Chem. Int. Ed.* **2010**, *49*, 7448–7451; *Angew. Chem.* **2010**, *122*, 7610–7613.
[5] D. N. Woodruff, R. E. P. Winpenny, R. A. Layfield, *Chem. Rev.* **2013**, *113*, 5110–5148.
[6] D. Gatteschi, R. Sessoli, *Angew. Chem. Int. Ed.* **2003**, *42*, 268–297; *Angew. Chem.* **2003**, *115*, 278–309.
[7] F. Troiani, M. Affronte, *Chem. Soc. Rev.* **2011**, *40*, 3119–3129.
[8] R. Sessoli, D. Gatteschi, A. Caneschi, M. A. Novak, *Nature* **1993**, *365*, 141–143.
[9] W. T. Carnall, P. R. Fields, B. G. Wybourne, *J. Chem. Phys.* **1965**, *42*, 3797.
[10] Y. Rechkemmer, J. E. Fischer, R. Marx, M. Dörfel, P. Neugebauer, S. Horvath, M. Gysler, T. Brock-Nannestad, W. Frey, M. F. Reid, J. van Slageren, *J. Am. Chem. Soc.* **2015**, *137*, 13114–13120.
[11] K. S. Pedersen, L. Ungur, M. Sigrist, A. Sundt, M. Schau-Magnussen, V. Vieru, H. Mutka, S. Rols, H. Weihe, O. Waldmann, L. F. Chibotaru, J. Bendix, J. Dreiser, *Chem. Sci.* **2014**, *5*, 1650–1660.
[12] R. Marx, F. Moro, M. Dörfel, L. Ungur, M. Waters, S. D. Jiang, M. Orlita, J. Taylor, W. Frey, L. F. Chibotaru, J. van Slageren, *Chem. Sci.* **2014**, *5*, 3287–3293.

These are not the final page numbers! ↗↗

[13] M. Perfetti, G. Cucinotta, M. E. Boulon, F. El Hallak, S. Gao, R. Sessoli, *Chem. Eur. J.* **2014**, *20*, 14051 – 14056.

[14] M. Gysler, F. El Hallak, L. Ungur, R. Marx, M. Hakl, P. Neugebauer, Y. Rechkemmer, Y. Lan, I. Sheikin, M. Orlita, C. E. Anson, A. K. Powell, R. Sessoli, L. F. Chibotaru, J. van Slageren, *Chem. Sci.* **2016**, *7*, 4347 – 4354.

[15] J. J. Baldoví, S. Cardona-Serra, J. M. Clemente-Juan, E. Coronado, A. Gaita-Ariño, A. Palii, *Inorg. Chem.* **2012**, *51*, 12565 – 12574.

[16] H. Bethe, *Ann. Phys.* **1929**, *395*, 133 – 208.

[17] P. Porcher, M. C. Dos Santos, O. Malta, *Phys. Chem. Chem. Phys.* **1999**, *1*, 397 – 405.

[18] W. Urland, *Chem. Phys.* **1976**, *14*, 393 – 401.

[19] C. K. Jorgensen, R. Pappalardo, H. H. Schmidtke, *J. Chem. Phys.* **1963**, *39*, 1422 – 1430.

[20] O. L. Malta, *Chem. Phys. Lett.* **1982**, *87*, 27 – 29.

[21] O. L. Malta, *Chem. Phys. Lett.* **1982**, *88*, 353 – 356.

[22] J. J. Baldoví, J. J. Borrás-Almenar, J. M. Clemente-Juan, E. Coronado, A. Gaita-Ariño, *Dalton Trans.* **2012**, *41*, 13705 – 13710.

[23] J. Ruiz, A. J. Mota, A. Rodríguez-Diéguez, S. Titos, J. M. Herrera, E. Ruiz, E. Cremades, J. P. Costes, E. Colacio, *Chem. Commun.* **2012**, *48*, 7916 – 7918.

[24] D. Aravena, E. Ruiz, *Inorg. Chem.* **2013**, *52*, 13770 – 13778.

[25] S. Gómez-Coca, D. Aravena, R. Morales, E. Ruiz, *Coord. Chem. Rev.* **2015**, *289*, 379 – 392.

[26] a) E. Moreno Pineda, N. F. Chilton, R. Marx, M. Dörfel, D. O. Sells, P. Neugebauer, S.-D. Jiang, D. Collison, J. van Slageren, E. J. L. McInnes, R. E. P. Winpenny, *Nat. Commun.* **2014**, *5*, 5243; b) D. Aravena, M. Atanasov, F. Neese, *Inorg. Chem.* **2016**, *55*, 4457 – 4469.

[27] D. H. Metcalf, T. A. Hopkins, F. S. Richardson, *Inorg. Chem.* **1995**, *34*, 4868 – 4878.

[28] K. A. Schoene, J. R. Quagliano, F. S. Richardson, *Inorg. Chem.* **1991**, *30*, 3803 – 3812.

[29] A. Lennartson, M. Hakansson, *CrystEngComm* **2009**, *11*, 1979 – 1986.

[30] L. F. Chibotaru, L. Ungur, *J. Chem. Phys.* **2012**, *137*, 064112.

[31] F. Aquilante, L. De Vico, N. Ferré, G. Ghigo, P.-Å. Malmqvist, P. Neogrády, T. B. Pedersen, M. Pitoňák, M. Reiher, B. O. Roos, L. Serrano-Andrés, M. Urban, V. Veryazov, R. Lindh, *J. Comput. Chem.* **2010**, *31*, 224.

[32] M. J. Frisch, G. W. Trucks, H. B. Schlegel, G. E. Scuseria, M. A. Robb, J. R. Cheeseman, G. Scalmani, V. Barone, B. Mennucci, G. A. Petersson, H. Nakatsuji, M. Caricato, X. Li, H. P. Hratchian, A. F. Izmaylov, J. Bloino, G. Zheng, J. L. Sonnenberg, M. Hada, M. Ehara, K. Toyota, R. Fukuda, J. Hasegawa, M. Ishida, T. Nakajima, Y. Honda, O. Kitao, H. Nakai, T. Vreven, J. A. Montgomery, Jr., J. E. Peralta, F. Ogliaro, M. Bearpark, J. J. Heyd, E. Brothers, K. N. Kudin, V. N. Staroverov, R. Kobayashi, J. Normand, K. Raghavachari, A. Rendell, J. C. Burant, S. S. Iyengar, J. Tomasi, M. Cossi, N. Rega, N. J. Millam, M. Klene, J. E. Knox, J. B. Cross, V. Bakken, C. Adamo, J. Jaramillo, R. Gomperts, R. E. Stratmann, O. Yazyev, A. J. Austin, R. Cammi, C. Pomelli, J. W. Ochterski, R. L. Martin, K. Morokuma, V. G. Zakrzewski, G. A. Voth, P. Salvador, J. J. Dannenberg, S. Dapprich, A. D. Daniels, Ö. Farkas, J. B. Foresman, J. V. Ortiz, J. Cioslowski, D. J. Fox, *Gaussian 09*, revision A.02, Gaussian, Inc., Wallingford, CT, **2009**.

[33] a) J. J. Baldoví, S. Cardona-Serra, J. M. Clemente-Juan, E. Coronado, A. Gaita-Ariño, A. Palii, *J. Comput. Chem.* **2013**, *34*, 1961 – 1967; b) J. J. Baldoví, J. M. Clemente-Juan, E. Coronado, A. Gaita-Ariño, A. Palii, *J. Comput. Chem.* **2014**, *35*, 1930 – 1934.

[34] J. J. Baldoví, E. Coronado, A. Gaita-Ariño, *Dalton Trans.* **2015**, *44*, 12535 – 12538.

[35] J. J. Baldoví, J. M. Clemente-Juan, E. Coronado, Y. Duan, A. Gaita-Ariño, C. Giménez-Saiz, *Inorg. Chem.* **2014**, *53*, 9976 – 9980.

[36] J. D. Rinehart, J. R. Long, *Chem. Sci.* **2011**, *2*, 2078 – 2085.

[37] H. Schilder, H. Lueken, *J. Magn. Magn. Mater.* **2004**, *281*, 17 – 26.

[38] S. T. Liddle, J. van Slageren, *Chem. Soc. Rev.* **2015**, *44*, 6655 – 6669.

↖↖ These are not the final page numbers!

J. J. Baldoví, Y. Duan, R. Morales, A. Gaita-Ariño, E. Ruiz,* E. Coronado*

■■ – ■■

Rational Design of Lanthanoid Single-Ion Magnets: Predictive Power of the Theoretical Models

Benchmarking predictive capabilities: Ab initio complete active space (CASSCF and CASPT2) and *semiempirical* radial effective charge (REC) theoretical methods are tested on a family of lanthanoid oxydiacetate single-ion magnets (see figure). Comparison of their predictions concerning energy levels, wave functions and magnetic properties with detailed spectroscopic and magnetic characterisation is used to critically discuss their performances.